LIOUVILLE-SPACE PATHWAYS AND PHASE-SPACE WAVEPACKETS IN FEMTOSECOND SPECTROSCOPY

SHAUL MUKAMEL
Chemistry Department, University of Rochester
Rochester, New York 14627-0216, USA

Abstract

The density matrix approach, which offers a physically transparent and numerically effective method for calculating optical signals and relating them to the underlying microscopic molecular motions, is surveyed. Nonlinear response functions combined with Wigner phase-space wavepackets provide a systematic classification of femtosecond techniques and allow a unified description of gas-phase and condensed-phase measurements. Applications to pump-probe, fluorescence and photon-echo spectroscopies are discussed.

I. Introduction

The radiation field interacts with molecular systems via the dipole operator V

$$H_{int} = - V \cdot E(t). \quad (1)$$

Consequently, optical spectroscopy, be it time-domain or frequency-domain, views the electronic and nuclear molecular dynamics through the time-dependent polarization (the expectation value of the dipole operator)

$$P(t) \equiv \langle \psi(t) | V | \psi(t) \rangle. \quad (2)$$

Calculations of the polarization are usually based on the time-dependent wavefunction $|\psi(t)\rangle$, representing the molecule driven by the external field(s). Spectroscopic techniques can be classified according to their order with respect to the incoming fields. To n'th order we have [1]

$$P^{(n)}(t) = \sum_{j=0}^{n} \langle \psi^{(j)}(t | V |) \psi^{(n-j)}(t) \rangle, \quad (3)$$

where $|\psi^{(j)}\rangle$ is the wavefunction expanded to j'th order. For example, linear absorption is related to $P^{(1)}$, whereas many common techniques such as pump-probe, four wave mixing, photon echo, fluorescence, hole burning, and coherent Raman measurements are related to $P^{(3)}$. The wavefunction is frequently used also to visualize the optical response in terms of time-dependent wavepackets. The traditional interpretation of optical measurements is therefore based on *amplitudes* ; the wavefunction $|\psi(t)\rangle$ is the amplitude of a material wave and E(t) is the field amplitude.

In this article we review an alternative approach for the theoretical analysis of femtosecond nonlinear spectroscopies which avoids the use of amplitudes, and focuses instead on dynamical quantities which more closely resemble the experimental

To appear in the proceedings of the
Nobel Symposium on Femtochemistry,
Stockholm, 1996
Ed. V. Sundström

Imperial College Press

observables and lend themselves more easily to semiclassical interpretations. The method is based on a density matrix representation of molecular dynamics [2-7] and Wigner spectrograms for the radiation fields [8-10]. The state of a molecule which has a probability P_α to be found in a state $|\psi_\alpha(t)\rangle$, is represented by the density matrix [11-13]

$$\rho(t) = \sum_\alpha P_\alpha |\psi_\alpha(t)\rangle \langle\psi_\alpha(t)|. \tag{4}$$

The polarization (eq. (3)) is then given by

$$P^{(n)}(t) = \mathrm{Tr}\,[V\,\rho^{(n)}(t)]. \tag{5}$$

The time evolution of the wavefunction is determined by the Schrodinger equation

$$\frac{d\psi}{dt} = -\frac{i}{\hbar} H\psi. \tag{6a}$$

Similarly, the evolution of the density matrix is given by the Liouville equation

$$\frac{d\rho}{dt} = -\frac{i}{\hbar}[H,\rho] \equiv -\frac{i}{\hbar} L\,\rho \tag{6b}$$

The second identity defines the Liouville operator L. Eqs. (6a) and (6b) are formally identical: The time evolution of a vector (ψ or ρ)is given by a matrix (H or L) times that vector. The difference is in the dimensionality of space: if ψ has N components, then ρ will have N^2 elements. ψ is a vector in *Hilbert space* where operators (such as H) are N x N matrices; ρ is a vector in *Liouville space* where operators (such as L) are N^2 x N^2 matrices. Liouville-space operators are also denoted superoperators.

In the Liouville space analysis, the density matrix $\rho(\mathbf{x}, \mathbf{x}')$ (or equivalently its Wigner transform $\rho(\mathbf{p}, \mathbf{q})$ [14], which represents a distribution in phase space) assumes the role of the wavefunction $\psi(\mathbf{x})$. Similarly, we replace the time-dependent fields $E_j(t)$ by their spectrograms $W_j(t,\omega)$ which reflect their joint temporal and spectral profiles [8-10]. At first glance it may seem that such representations add a layer of complexity to the theoretical analysis; since we double the space (function of t and ω rather than t for the field and function of $\mathbf{x}\,\mathbf{x}'$ rather than for $\mathbf{x}$ the molecule). However, the vantage point of Liouville space offers a bird's eye view which carries tremendous conceptual as well as practical computational advantages, as will be demonstrated in this article: The bookkeeping of time ordering of the various interactions with the radiation field provides a physically transparent description in terms of Liouville space pathways. Intuitive semiclassical approximations can be developed using wavepackets in phase space corresponding to the density matrix in the Wigner representation, and correlation function expressions for optical signals establish the connections among various nonlinear techniques and their information content. In addition, the proper description of spontaneous emission in, e.g., fluorescence spectroscopy requires a correlation function treatment and may not be formulated using the time-dependent wavefunction All of these advantages apply to

any molecular system ranging from isolated small molecules [15,16] all the way to complex molecules in condensed phase [17-19]. For large molecules at finite temperatures, the density matrix has additional merits; in eq. (4), if $P_\alpha = 1$ for one state and $P_\alpha = 0$ otherwise, the molecule can be represented by a wavefunction; this is a quantum mechanical *pure state* with complete information. Otherwise the molecule is in a *mixed state* or a statistical mixture. In that case we can no longer represent it by a single wavefunction, but we can still do that with a single density matrix!. In the Liouville space form we calculate directly the thermally averaged signal by propagating a density matrix representing a mixed state (rather than a pure state). No further averaging over thermal distributions is necessary. Furthermore, in the condensed phase we must develop a reduced description in which we follow explicitly only the dynamics of a few selected and relevant degrees of freedom; the remaining degrees of freedom are treated as a thermal bath and are eliminated from the description. The bath may consist of some intermolecular vibrational degrees of freedom weakly coupled to the electronic transition, solvent degrees of freedom, optical and acoustic phonons in crystals, local modes for impurity spectra, etc. The density matrix offers a practical way for developing a reduced description, and allows us to perform all the necessary averagings directly [13,20]. Using the wavefunction we have to consider each member of the ensemble, calculate its dynamics, and average the result at the end. When this is done, we find that the effects of the bath on the various Liouville space pathways are profoundly different. These effects can be interpreted naturally by introducing the concept of dephasing processes (which is not possible in a wavefunction description).

In the following sections we survey the main ideas behind the Liouville space approach to nonlinear spectroscopy and illustrate its merits in the analysis of pump-probe, fluorescence and multidimensional photon echo techniques.

II. Correlation-function expressions for pump-probe spectroscopy

The electric field corresponding to the incoming laser pulses in nonlinear spectroscopy may be represented in the form.

$$E(t) = \sum_j \left[E_j(t) \exp\left(-i\,\omega_j t + i\,\mathbf{k}_j\cdot\mathbf{r}\right) + E_j^*(t) \exp\left(i\,\omega_j t - i\,\mathbf{k}_j\cdot\mathbf{r}\right) \right]. \qquad (7)$$

Here $E_j(t)$ is the complex amplitude (analytical signal) of the j'th field with central frequency ω_j and wavevector $\mathbf{k}_j$. A different representation of the field which is more adequate for the interpretation of nonlinear measurements is provided by its *Wigner spectrogram* [8-10]

$$W_j(t,\omega) = \int_{-\infty}^{\infty} E_j^*(t - \tau/2)\, E_j(t + \tau/2) \exp(i\omega\tau)\, d\tau. \qquad (8)$$

This function gives the joint spectral and temporal profile of the j'th field. Unlike the field itself, it can be measured by nonlinear correlation techniques. Its temporal (spectral) integrals give the spectral (temporal) profile of the field:

$$\int \frac{d\omega}{2\pi} W_j(t,\omega) = |E_j(t)|^2 \quad ; \quad \int dt\, W_j(t,\omega) = |E_j(\omega)|^2. \tag{9}$$

We now consider an experiment in which the molecule is subjected to an arbitrary number of pulses, and its dynamics is finally monitored through the absorption of a weak probe field (E_2).* The absorption rate is then given by [21]

$$S_{probe} = \mathrm{Im} \int_{-\infty}^{\infty} E_2^*(t)\, P(t)\, dt \tag{10}$$

Since the probe is weak, we can expand the polarization P(t) to linear order in E_2, and obtain

$$S_{probe} = \mathrm{Im} \int_{-\infty}^{\infty} dt \int_{-\infty}^{t} d\tau\, E_2^*(t)\, E_2(\tau) \left\langle \frac{i}{\hbar} [\tilde{V}(t), \tilde{V}(\tau)] \right\rangle. \tag{11}$$

Here $\tilde{V}(\tau)$ is the polarization evolving in time with the Hamiltonian which excludes the probe (but includes all other fields). The angular brackets in this article imply an expectation value with respect to the equilibrium density matrix ρ_{eq}; i.e.,

$$\langle [\tilde{V}(t), \tilde{V}(\tau)] \rangle \equiv \mathrm{Tr}\{[\tilde{V}(t), \tilde{V}(\tau)]\rho_{eq}\}. \tag{12}$$

This form allows us to separate the roles of the probe from the other fields. The probe absorption may be recast in the form [10]

$$S_{probe} = \int dt \int \frac{d\omega}{2\pi} W_2(t,\omega)\, S_0(t,\omega), \tag{13a}$$

where W_2 is the Wigner spectrogram of the E_2 field, and

$$S_0(t,\omega) = \mathrm{Im} \int_0^{\infty} d\tau\, \exp(i\omega\tau) \left\langle \frac{i}{\hbar} [\tilde{V}(t + \tau/2), \tilde{V}(t - \tau/2)] \right\rangle, \tag{13b}$$

is the snapshot absorption profile.

The following limits are obtained naturally from this result. If the probe is impulsive (short), compared with nuclear dynamics, we obtain the time-resolved spectrum.

$$S_{probe}(t) = \int \frac{d\omega}{2\pi} S_0(t,\omega). \tag{14a}$$

---

* The following results apply, with minor modifications, to any type of heterodyne detected four-wave mixing.

In the opposite limit of spectrally-narrow pulse, we obtain the frequency-domain spectrum

$$S_{probe}(\omega) = \int dt\, |E_2(t)|^2\, S_0(t,\omega). \tag{14b}$$

Assuming a pump-probe measurement conducted with a weak pump and a weak probe, we can expand eq. (13b) to second order in the pump. We further assume that the pump and the probe are well separated temporally. This gives*

$$S_{pp} = \mathrm{Im}\left(\frac{i}{\hbar}\right)^3 \int_{-\infty}^{\infty} dt \int_{-\infty}^{t} d\tau_3 \int_{-\infty}^{\infty} d\tau_2 \int_{-\infty}^{\tau_2} d\tau_1$$

$$\langle [V(t), V(\tau_3)]\, [V(\tau_2), [V(\tau_1), \rho_{eq}]\,]\rangle\; E_2^*(t)\, E_2(\tau_3)\, E_1^*(\tau_2)\, E_1(\tau_1) \tag{15}$$

Here the time-dependence of V(t) is determined by the purely molecular Hamiltonian (H) with no fields

$$V(t) = \exp\left(\frac{i}{\hbar}Ht\right) V \exp\left(-\frac{i}{\hbar}Ht\right). \tag{16}$$

The upper limit of the τ_2 integration was changed from τ_3 to ∞; this is justified when the pulses are well separated. This result can be recast in the form

$$S_{pp} = \int\int\int\int \frac{d\omega_1}{2\pi}\frac{d\omega_2}{2\pi}\, dt_1\, dt_2\, W_2(\omega_2, t_2)\, S^0_{pp}(\omega_2, t_2; \omega_1, t_1)\, W_1(\omega_1, t_1)$$

with (17a)

$$S^0_{pp}(\omega_2, t_2; \omega_1, t_1) = \mathrm{Im}\left(\frac{i}{\hbar}\right)^3 \int_0^{\infty} d\tau_1 \int_0^{\infty} d\tau_2 \exp(i\omega_1\tau_1 + i\,\omega_2\tau_2)$$

$$\langle [V(t_2 + \tau_2/2), V(t_2 - \tau_2/2)] \cdot [V(t_1 + \tau_1/2), [V(t_1 - \tau_1/2), \rho_{eq}]\,]\rangle. \tag{17b}$$

S^0_{pp} is an ideal *snapshot spectrum* corresponding to pump and probe with sharply defined frequency and time. It contains all the molecular information necessary for the analysis of measurements conducted with realistic pulses. The actual signal is obtained by convoluting the snapshot spectrum with the pump and the probe spectrograms, defined in eq. (8). In this form the roles of the spectral and temporal profiles of the pulses and of the molecular response are clearly separated.

The molecular information in eqs. (17) (as in all nonlinear optical measurement) is expressed as a combination of the n point correlation functions of the

---

* Eq. (15) can be obtained directly from eq. (10) by expanding the polarization to third order in the fields (second order in the pump, first order in the probe), using eqs. (30). In eqs. (15) and (17b) ρ_{eq} is written explicitly and the angular bracket simply denotes a trace (unlike eq. (12)).

dipole operator $\langle V(\tau_1)\, V(\tau_2) \ldots V(\tau_n)\rangle$. At this point, we can expand these correlation functions in molecular eigenstates and obtain

$$\langle V(\tau_1)\, V(\tau_2)\rangle = \sum_{a,b} P(a)\,|V_{ab}|^2 \exp[-i\omega_{ba}(\tau_2 - \tau_1)] \tag{18a}$$

$$\langle V(\tau_1)\, V(\tau_2)\, V(\tau_3)\, V(\tau_4)\rangle$$
$$= \sum_{a,b,c,d} P(a)\, V_{ab} V_{bc} V_{cd} V_{da} \exp(-i\omega_{ba}\tau_1 - i\omega_{cb}\tau_2 - i\omega_{dc}\tau_3 - i\omega_{ad}\tau_4) \tag{18b}$$

where $\omega_{jj'} \equiv \varepsilon_j - \varepsilon_{j'}$ are the transition frequencies between pairs of eigenstates. Doing so, we recover the conventional expression for the signal calculated using the wavefunction approach. However, the power of the correlation function formalism is that it enables us to avoid these summations altogether and to derive alternative expressions which use, e.g., wavepackets in phase space or semiclassical simulation techniques. These will be demonstrated in the coming sections.

III. Wavepackets in phase space: The doorway/window representation of pump-probe spectroscopy

The density matrix and the Liouville equation are well rooted in Classical statistical mechanics. One of the major advantages of working in Liouville space is the existence of a well defined classical limit for all quantities. This is to be contrasted with the wavefunction which does not have a classical counterpart. In this section we introduce the Wigner representation which provides a powerful semiclassical picture that interpolates between the classical and the quantum limits. We start by expressing the density matrix in the *coordinate representation*

$$\langle \mathbf{x}\,|\,\rho(t)\,|\,\mathbf{x}'\rangle \equiv \rho(\mathbf{x},\mathbf{x}',t) \equiv \sum_{nm} \rho_{nm}\psi_n(\mathbf{x})\psi_m^*(\mathbf{x}') \tag{19}$$

where $\{|\psi_n\rangle\}$ is an arbitrary basis set and $\mathbf{x}$ is an N dimensional vector representing the molecular coordinates. The Wigner representation of the density matrix is defined through the Fourier transform [14]

$$\rho_W(\mathbf{q},\mathbf{p};t) = \frac{1}{(2\pi\hbar)^N} \int_{-\infty}^{\infty} \langle\, \mathbf{q} + \mathbf{s}/2\,|\,\rho(t)\,|\,\mathbf{q} - \mathbf{s}/2\rangle \exp\left(-\frac{i}{\hbar}\,\mathbf{p}\cdot\mathbf{s}\right) d\mathbf{s}, \tag{20a}$$

where $\mathbf{q} = (\mathbf{x} + \mathbf{x}')/2$ is the mean coordinate, whereas $\mathbf{p}$ is the momentum conjugate to $\mathbf{s} \equiv \mathbf{x} - \mathbf{x}'$. The Wigner representation $A_W(\mathbf{q},\mathbf{p})$ of an arbitrary operator A is similarly defined by

$$A_W(\mathbf{q},\mathbf{p};t) = \int_{-\infty}^{\infty} \langle\, \mathbf{q} + \mathbf{s}/2\,|\,A(t)\,|\,\mathbf{q} - \mathbf{s}/2\rangle \exp\left(-\frac{i}{\hbar}\,\mathbf{p}\cdot\mathbf{s}\right) d\mathbf{s} \tag{20b}$$

(Note that the $(2\pi\hbar)^{-N}$ prefactor is omitted here.) Using these definitions, the expectation value of an arbitrary dynamical variable A is given by

$$\langle A(t)\rangle \equiv \mathrm{Tr}[A\rho(t)] = \int_{-\infty}^{\infty}\int_{-\infty}^{\infty} dx dx'\, A(x',x)\rho(x,x';t)$$

$$= \int_{-\infty}^{\infty}\int_{-\infty}^{\infty} dp\, dq\, A_W(pq)\,\rho_W(pq;t) \qquad (21)$$

We shall view this as the expectation value in the *Wigner representation.* In classical statistical mechanics we describe the evolution of a system in *phase space* whose coordinates are the positions **q** and the momenta **p** of all particles. The state of the system with complete information may be represented by a point in phase space. More generally, a classical system is represented by a distribution function in phase space, and the expectation value of any dynamical variable is calculated by a phase space average, analogous to the second equality in eq. (21). Note, however, that despite its classical appearance, the phase space average in eq. (21) retains the full quantum characteristics of the system. In the Wigner representation, the density matrix as well as any other operator are represented by a complex function of phase space. When $\hbar \to 0$ the Wigner density matrix ρ_w reduces to the classical distribution and the classical limit is recovered. As an example, consider a quantum harmonic oscillator with frequency ω and mass m. Its canonical density matrix in the Wigner representation is

$$\rho_w(p,q) = \frac{1}{2\pi\sigma_p\sigma_q}\exp\left[\frac{p^2}{2\sigma_p^2} - \frac{q^2}{2\sigma_q^2}\right] \qquad (22a)$$

with

$$\sigma_p^2 = 2m\sigma;\quad \sigma_q^2 = \frac{2\sigma}{m\omega^2};\quad \sigma \equiv \frac{1}{2}\hbar\omega\coth(\beta\hbar\omega/2) \qquad (22b)$$

At low temperatures $(\beta\hbar\omega >> 1)$ we have $\sigma = \frac{1}{2}\hbar\omega$. ρ_w is then the Wigner transform of the ground state of the harmonic oscillator. In the opposite, high temperature limit $(\beta\hbar\omega << 1)$ we have $\sigma = k_BT$. ρ_w is then simply equal to the classical canonical distribution function of the harmonic oscillator, which does not depend on $\hbar$. At high temperatures ρ_w is classical, as required by the correspondence principle. At low temperatures, however, the classical distribution function has a zero width $\sigma_p = \sigma_q = 0$, whereas the Wigner function has a width corresponding to the zero point motion.

Making use of the Wigner representation, we can recast the pump-probe spectrum using wavepackets in phase space [20,21]. We assume a two electronic level system with ground a state $|g\rangle$ and an excited state $|e\rangle$. Eq. (17a) then becomes

$$S_{pp} = \int\int \mathbf{dp\,dq} \int\int \mathbf{dp'\,dq'}\,[\mathcal{W}_g(\mathbf{pq})\,G_g(\mathbf{pq}\tau;\,\mathbf{p'q'})\,\mathcal{D}_g(\mathbf{p'q'})$$

$$+\,\mathcal{W}_e(\mathbf{pq})\,G_e(\mathbf{pq}\tau;\,\mathbf{p'q'})\,\mathcal{D}_e(\mathbf{p'q'})]. \qquad (23)$$

The *doorway wavepackets* are given by

$$\mathcal{D}_n\,\mathbf{p'q'} = \iint dt_1\,d\omega_1\,\mathcal{D}_n^0(\mathbf{p'q'};t_1\omega_1)\,W_1(t_1\omega_1) \qquad n = g,e\ , \qquad (24a)$$

with the snapshot doorway

$$\mathcal{D}_e^0(\mathbf{p'q'};\,t_1\omega_1)$$

$$= \int_{-\infty}^{\infty} d\tau_1 \int\int d\mathbf{x}\,d\mathbf{x'}\,\langle\mathbf{x'}|\,V_{eg}(t_1+t_1/2)\,\rho_{eq}V_{ge}(t_1-t_1/2)\,|\mathbf{x}\rangle$$

$$\times\ \delta(2\mathbf{q'}-\mathbf{x}-\mathbf{x'})\exp[i\mathbf{p'}(\mathbf{x}-\mathbf{x'})+i\omega_1\,\tau_1], \qquad (24b)$$

$$\mathcal{D}_g^0(\mathbf{p'q'};\,t_1\omega_1)$$

$$= \int_{-\infty}^{\infty} d\tau_1 \int\int d\mathbf{x}\,d\mathbf{x'}\,\langle\mathbf{x'}|\,V_{ge}(t_1+\tau/2)\,V_{eg}(t_1-\tau/2)\rho_{eq}\,|\mathbf{x}\rangle$$

$$\times\ \delta(2\mathbf{q'}-\mathbf{x}-\mathbf{x'})\exp[i\mathbf{p'}(\mathbf{x}-\mathbf{x'})+i\omega_1\,\tau_1]. \qquad (24c)$$

The *window wavepackets* are given by

$$\mathcal{W}_n(\mathbf{pq}) = \iint dt_2\,d\omega_2\ \mathcal{W}_n^0(\mathbf{pq};\,t_2\,\omega_2)\,W_2(t_2\,\omega_2) \qquad n = g,e\ , \qquad (25a)$$

with the snapshot window

$$\mathcal{W}_g^0(\mathbf{pq};\,t_2\,\omega_2) = \int_{-\infty}^{\infty} d\tau_2 \iint d\mathbf{x}\,d\mathbf{x'}\langle\mathbf{x'}|\,V_{ge}(t_1+\tau_1/2)\,V_{eg}(t_1-\tau_1/2)\,|\mathbf{x}\rangle$$

$$\times\ \delta(2\mathbf{q}-\mathbf{x}-\mathbf{x'})\exp[i\mathbf{p}(\mathbf{x}-\mathbf{x'})+i\omega_2 t_2]\,, \qquad (25b)$$

$$\mathcal{W}_e^0(\mathbf{pq};\,t_2\,\omega_2) = \int_{-\infty}^{\infty} d\tau_2 \iint d\mathbf{x}\,d\mathbf{x'}\langle\mathbf{x'}|\,V_{eg}(t_1+\tau_1/2)\,V_{ge}(t_1-\tau_1/2)\,|\mathbf{x}\rangle$$

$$\times\ \delta(2\mathbf{q}-\mathbf{x}-\mathbf{x'})\exp[i\mathbf{p}(\mathbf{x}-\mathbf{x'})+i\omega_2 t_2]\,. \qquad (25c)$$

Eqs. (23-25) offer the following physical picture of the pump-probe spectrum [6]. The pump transfers a fraction of the molecules from the ground state to the excited

state, thus creating an excited state "particle" wavepacket $\mathcal{D}_e$ and a ground state "hole" $\mathcal{D}_g$. Similarly, the probe creates two window wavepackets in the excited state ($\mathcal{W}_e$) and in the ground state ($\mathcal{W}_g$). $G_n(\mathbf{pq}\tau; \mathbf{p'q'})$ Is the propagator from phase space point $\mathbf{p'q'}$ to $\mathbf{pq}$ during the time τ (the delay between the pump and the probe) in the n'th electronic state n = g,e. The probe absorption has two contributions: the hole contribution is obtained by taking the ground state doorway $\mathcal{D}_g$, propagating it for the delay period and then calculating its phase space overlap with the window $\mathcal{W}_g$. The second (particle) contribution is similar, except that the time evolution is now in the excited state. These results provide an intuitive interpretation of pump-probe measurements: the calculation has been naturally separated into preparation, evolution, and detection stages. Furthermore, this form shows clearly how the time-frequency uncertainty for the field and the coordinate-momentum uncertainty of the molecular coordinates affect the signal. Despite its classical form, this is a fully quantum mechanical expression, since the Wigner wavepackets retain the quantum nature of the system. The important point is that we can discuss quantum and classical systems using the same language, and the wavepackets will become classical when appropriate. The only approximation made in the derivation of eq. (23) is the assumption that the two pulses are well separated. When this is not the case, the doorway/window phase space representation can still be used; however, additional contributions should be included in the response [7].

IV. Nuclear wavepackets for time-and frequency-resolved fluorescence

Measurements involving spontaneous light emission such as Raman and fluorescence spectroscopy cannot be expressed in terms of expectation values of molecular operators; they require a two-time correlation function of the driven system, which may not be calculated using $|\psi(t)\rangle$.*

In general, the time- and frequency-resolved spontaneous emission spectrum is given by [23]

$$S(t,\omega) = \int_{-\infty}^{\infty} d\tau \langle \tilde{V}_-(t - \tau/2)\, \tilde{V}_+(t + \tau/2) \rangle \exp(i\omega\tau), \qquad (26)$$

where $\tilde{V}_+$ ($\tilde{V}_-$) is the positive (negative) frequency part of the dipole operator of the molecule driven by the external field. By expanding this expression to second order in the incoming field, the fluorescence spectrum is given by

---

* It is possible to express this spectrum using a single time expectation value, provided we treat the radiation field quantum mechanically [4,22].

$$S_{FI} = \int \int \int \int \frac{d\omega_1}{2\pi}\frac{d\omega_2}{2\pi} dt_1 dt_2 \, W_d(\omega_2 t_2) \, S^0_{FI}(\omega_2 t_2; \omega_1 t_1) \, W_1(\omega_1 t_1),$$

with the snapshot spectrum (27a)

$$S^0_{FI}(\omega_2; t_2; \omega_1; t_1)$$

$$= \int_{-\infty}^{\infty} d\tau_1 \int_{-\infty}^{\infty} d\tau_2 \langle V_{ge}(t_1 + \tau_1/2) \, V_{eg}(t_2 + \tau_2/2) \, V_{ge}(t_2 - \tau_2/2) \, V_{eg}(t_1 - \tau_1/2) \rangle$$

$$\exp(i\omega_1 \tau_1 + i\omega_2 \tau_2). \quad (27b)$$

Here, W_1 is the Wigner spectrogram of the incoming pump field, whereas W_d is a Wigner function representing the detection process and controlling its temporal and spectral resolution [10]. In complete analogy with our derivation of the pump probe spectrum (eq. (23)), we can recast this expression using phase-space wavepackets.

$$S_{FI} = \int \int d\mathbf{p}\, d\mathbf{q} \int \int d\mathbf{p}' d\mathbf{q}' \mathcal{W}_e(\mathbf{pq}) \, G_e(\mathbf{pq}; \mathbf{p}'\mathbf{q}'\, \tau) \, \mathcal{D}_e(\mathbf{p}'\mathbf{q}'). \quad (28)$$

The doorway wavepacket $\mathcal{D}_e(\mathbf{p}'\mathbf{q}')$ is given by eqs. (24). The window wavepacket $\mathcal{W}_e(\mathbf{pq})$ is similar to eqs. (25), except that the probe spectrogram $W_2(t_2\omega_2)$ is replaced by the detector function $W_d(t_2\omega_2)$. The latter is given by the convolution of its spectral and temporal transmission functions, and is centered around some specified time t_0 and frequency ω_0.

V. Liouville-space pathways for nonlinear response functions.

So far we have restricted our discussion to pump-probe spectroscopy which is conceptually the simplest ultrafast nonlinear technique. More generally, it is possible to analyze any optical measurement using *nonlinear response functions* obtained by expanding the polarization in powers of the incoming fields. To first order we have

$$P^{(1)}(t) = \int_{-\infty}^{\infty} d\tau \, S^{(1)}(t, \tau) \, E(\tau), \quad (29a)$$

with the linear response function

$$S^{(1)}(t, \tau) = i/\hbar \, \langle [V(t), V(\tau)] \rangle. \quad (29b)$$

The third order polarization is similarly given by

$$P^{(3)}(t) = \int_{-\infty}^{t} d\tau_3 \int_{-\infty}^{\tau_3} d\tau_2 \int_{-\infty}^{\tau_2} d\tau_1 \, S^{(3)}(t, \tau_3, \tau_2, \tau_1) \, E(\tau_1) E(\tau_2) E(\tau_3), \quad (30a)$$

with the third order response function

$$S^{(3)}(t, \tau_3, \tau_2, \tau_1) = (i/\hbar)^3 \langle [[[V(t), V(\tau_3)], V(\tau_2)], V(\tau_1)] \rangle. \quad (30b)$$

The response functions are combinations of correlation functions. The generalization of these results to an arbitrary n'th order response is straightforward: $S^{(n)}$ has 2^n terms corresponding to all "left" and "right" choices of the n commutators. It is possible to represent the various Liouville space paths using double-sided Feynman diagrams that maintain the bookkeeping of the "left" and "right" interactions and their relative time ordering. An example representing the three-pulse echo (which will be discussed in Sec. VII) is shown in Fig. 1.

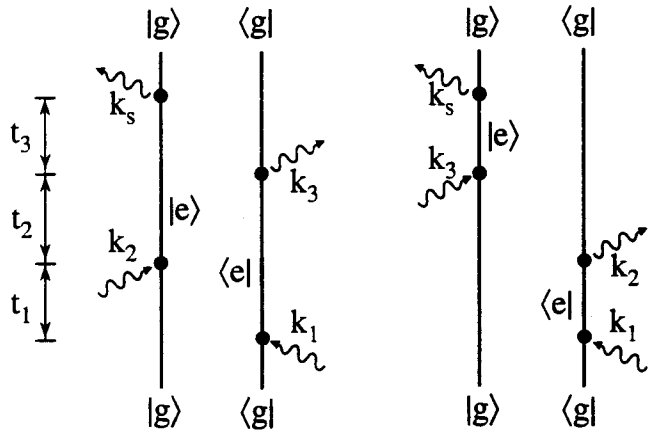

***Fig. 1** The two double-sided Feynman diagrams and Liouville space paths contributing to the three pulse photon echo in a two-level system in the rotating wave approximation.*

In the classical limit, the combination of correlation functions in $S^{(n)}$ behaves as $\sim\hbar^n$. The $\hbar^{-n}$ prefactor thus cancels and the classical response function which is independent of $\hbar$ is recovered [24]. The classical limit involves a delicate interference among the various Liouville space paths contributing to the response functions. Unlike the response functions, individual correlation functions do not have an obvious classical limit.

The nonlinear response functions can be applied to a broad range of nonlinear optical measurements which differ by the temporal sequences of pulses as well as their frequencies and wavevectors. The response functions allow us to calculate the signals and compare the information content of these techniques. Since the nonlinear response functions $S^{(n)}$ are successively probing higher order correlation functions, they necessarily carry more information as the order n is increased. The nonlinear response functions are expressed in terms of multitime molecular correlation functions, which provide a natural link between theory and experiment [25]. They can be formally defined without alluding to a particular technique, and consequently they

unify a large body of information and clarify the fundamental relationships among various techniques. In contrast, when calculating optical signals using wavefunctions, we need to repeat the calculation for each new technique. For example, the phenomenological description of hole burning and photon echo measurements is very different. However, using the correlation function approach, we can show that under some general conditions they are simply related by a Fourier transform. Physical observables are directly and linearly related to the density matrix. Consequently every step and intermediate quantity appearing in the density matrix description has a simple physical meaning and a well defined classical analogue. This is to be contrasted with wavefunction based theories which calculate a transition amplitude, which by itself is not an observable quantity. The signal is related to sums of products of such amplitudes. The time variables appearing in the expansion of the density matrix are completely chronologically ordered and represent the time intervals between successive interactions. In contrast, the time variables appearing when the wavefunction is expanded perturbatively in the fields are not fully ordered and consequently have a much less obvious physical interpretation. The complete and direct bookkeeping of time ordering makes the description using the density matrix most intuitive and directly relevant to experiment. Finally, since the Liouville space pathways are complex quantities, they may interfere when added. This interference results in some dramatic effects such as the generation of fluorescence, and extra resonances in four wave mixing [5,26].

Diagonal and off diagonal elements of the density matrix in a given basis set are known as populations and coherences, respectively. When an off diagonal element evolves in time, it acquires a phase since its evolution from the left (ket) and the right (bra) is governed by different Hamiltonians. This phase depends on the state of the bath. Performing an ensemble average over the distribution of bath degrees of freedom, this phase yields a damping of these elements. The damping of off diagonal elements of the density matrix resulting from phase (as opposed to amplitude) fluctuations is called dephasing or phase relaxation. Dephasing processes can be described only in Liouville space, where we distinguish between diagonal and off diagonal elements of the density matrix. We then follow simultaneously the evolution of the bra and of the ket and maintain the bookkeeping of their joint state. Dephasing processes directly affect spectroscopic observables. Since different Liouville-space pathways represent distinct sequences of populations an coherences, they will be affected differently by nuclear motions and dephasing processes. This further demonstrates the merits of Liouville space, where these terms are naturally separated. It should be emphasized that in a complete description of a system, where we follow explicitly the dynamics of all degrees of freedom, we do not need to invoke the concept of dephasing and a wavefunction description is in principle possible. However, this is impractical for realistic condensed-phase systems where a reduced description is essential. It is possible to calculate any physical process without ever introducing the concept of dephasing. However, it is hard to imagine our understanding of macroscopic reduced dynamics and its spectroscopic signatures without the notion of dephasing processes.

The wavepacket representation obtained earlier for pump-probe spectroscopy can be extended to the more general nonlinear response function. As can be seen from eq. (30b), $S^{(3)}$ has eight contributions. We shall label them $S_\alpha^{(3)}$ and write

$$S^{(3)}(t, \tau_3, \tau_2, \tau_1) = \sum_{\alpha=1}^{8} S_\alpha^{(3)}(t, \tau_3, \tau_2, \tau_1) . \tag{31a}$$

For each path α, we can calculate a complex phase-space wavepacket $\rho_\alpha^{(3)}$ representing its contribution to the total density matrix . We can then write

$$S_\alpha^{(3)}(t, \tau_3, \tau_2, \tau_1) = \mathrm{Tr}\left[V\rho_\alpha^{(3)}(t, \tau_3, \tau_2, \tau_1)\right] = \int\int \mathbf{dp}\, \mathbf{dq}\, V(\mathbf{q})\, \rho_\alpha^{(3)}(t, \tau_3, \tau_2, \tau_1; \mathbf{pq}) \tag{31b}$$

Each Liouville space path has its own density matrix. Examination of ρ_α provides an insight into the microscopic dynamics underlying each path. ρ_α may be calculated semiclassically using pairs of trajectories representing separately the bra and the ket during each evolution period [27].

VI. Solvent spectral densities and the multimode Brownian oscillator model

The molecular electronic states are coupled to a number of vibrational modes representing intramolecular vibrations, local intermolecular modes, as well as collective solvent modes. Nuclear motions may often be modeled as small amplitude harmonic vibrations whose equilibrium positions are displaced upon electronic excitation. Consider a molecule with two electronic levels; a ground state $|g\rangle$ and an excited state $|e\rangle$ with several nuclear coordinates q_j coupled linearly to the electronic system . The total Hamiltonian is given by

$$H = |g\rangle H_g \langle g| + |e\rangle(\hbar\omega_{eg}^0 + H_e)\langle e| + H' \tag{32a}$$

with

$$H_n = \sum_j \left[\frac{p_j^2}{2\mathcal{M}_j} + \frac{1}{2}\mathcal{M}_j\omega_j^2\left(q_j + d_j^{(n)}\right)^2\right], \qquad n = g,e \tag{32b}$$

p_j,q_j, and $\mathcal{M}_j$ represent the momentum, the coordinate and the mass, respectively, and $d_j^{(n)}$ is the equilibrium configuration. We further denote the relative displacement $d_j \equiv d_j^{(e)} - d_j^{(g)}$. In addition, these nuclear coordinates are coupled to a bath consisting of a set of harmonic oscillators with coordinates x_n and momenta p_n. The interaction between the system and the n'th bath oscillator is assumed to be linear with a coupling strength c_n. The coupling with the bath is described by the hamiltonian [20,28,29]

$$H' = \sum_n \left[\frac{p_n^2}{2m_n} + \frac{m_n \omega_n^2}{2} \left(x_n - \sum_j \frac{c_{nj} q_j}{m_n \omega_n^2} \right)^2 \right]. \tag{32c}$$

The total system is assumed to be initially at equilibrium in the ground electronic state.

All linear and nonlinear optical properties of this model are determined by the spectral function $g(t) = \sum_j g_j(t)$ with

$$g_j(t) = \frac{1}{2\pi} \int_{-\infty}^{\infty} d\omega \left(\frac{1 - \cos(\omega t)}{\omega^2} \right) \coth(\beta\hbar\omega/2) C_j''(\omega)$$

$$+ \frac{i}{2\pi} \int_{-\infty}^{\infty} d\omega \left(\frac{\sin(\omega t) - \omega t}{\omega^2} \right) C_j''(\omega), \tag{33a}$$

where the nuclear spectral density of the j'th nuclear mode is given by

$$C_j''(\omega) \equiv \eta_j \int_{-\infty}^{\infty} dt \exp(i\omega t) \left\langle \frac{i}{2} [q_j(t), q_j(0)] \right\rangle, \tag{33b}$$

with

$$\eta_j = \left(\frac{\mathcal{M}_j \omega_j^2 d_j}{\hbar} \right)^2. \tag{33c}$$

The choice of harmonic potentials allows the incorporation of a general model of dissipation with an arbitrary spectral density and temperature. The linear response is given by eq. (29b) with

$$\langle V(\tau_1) V(\tau_2) \rangle = \exp[-i\omega_{eg}(\tau_1 - \tau_2) - g(\tau_1 - \tau_2)]. \tag{34}$$

The third order response function is given by eq. (30b) with

$$\langle V(\tau_1) V(\tau_2) V(\tau_3) V(\tau_4) \rangle = \exp[-i\omega_{eg}(\tau_1 - \tau_2 + \tau_3 - \tau_4)]$$

$$\exp[-g(\tau_1 - \tau_2) + g(\tau_1 - \tau_3) - g(\tau_2 - \tau_3) - g(\tau_1 - \tau_4) + g(\tau_2 - \tau_4) - g(\tau_3 - \tau_4)]. \tag{35}$$

Upon the substitution of the proper time arguments (eq. (35)) in eq. (30b), we obtain the third order response function.

For the present model, the spectral density is given by

$$C_j''(\omega) = \frac{\hbar \eta_j}{\mathcal{M}_j} \frac{\omega \gamma_j(\omega)}{(\omega^2 - \omega_j^2)^2 + \omega^2 \gamma_j^2(\omega)}, \tag{36a}$$

where $\gamma_j(\omega)$ is related to the spectral distribution of the coupling,

$$\gamma_j(\omega) = \frac{\pi}{\mathcal{M}_j} \sum_n \frac{c_{nj}^2}{2m_n \omega_n^2} [\delta(\omega - \omega_n) - \delta(\omega + \omega_n)]. \tag{36b}$$

The frequency dependence of $\gamma_j(\omega)$ reflects the timescales of thermal motions of the bath. Assuming that these motions are very fast compared with the oscillator motion we can set $\gamma_j(\omega) = \gamma$ independent on ω. A general expression for g(t) calculated using the spectral density (36) is given in [2]. In the following we consider a few limiting cases where the optical response functions greatly simplify. We consider first the isolated molecule without a bath. Setting $H' = 0$, the spectral density becomes

$$C_j''(\omega) = 2\pi \sum_j S_j \omega_j^2 \; [\delta(\omega-\omega_j) - \delta(\omega+\omega_j)], \tag{37a}$$

where we have introduced the Huang-Rhys factor $S_j \equiv \frac{\mathcal{M}_j \omega_j d_j^2}{2\hbar}$. This results in the following expression for the line broadening function

$$g(t) = \sum_j S_j \left[(\coth(\beta\hbar\omega_j/2)\left(1 - \cos\left(\omega_j t\right)\right) + i\left(\sin(\omega_j t) - \omega_j t\right)\right] \tag{37b}$$

The absorption lineshape is given by

$$\sigma_a(\omega) = \frac{1}{\pi} \mathrm{Re} \int_0^\infty dt \exp[i(\omega-\omega_{eg})t - g(t)], \tag{38a}$$

and the relaxed fluorescence spectrum is

$$\sigma_f(\omega) = \frac{1}{\pi} \mathrm{Re} \int_0^\infty dt \exp[i(\omega-\omega_{eg} + 2\lambda)\, t - g^*(t)], \tag{38b}$$

with $\lambda = \sum_j \lambda_j$ and $\lambda_j = \omega_j S_j$. The first moment of σ_a vanishes, whereas the first moment of σ_f is $- 2\lambda$. For the present model σ_f is the mirror image of σ_a around $\omega_{eg}^0 = \omega_{eg} - \lambda$. For a single mode at zero temperature, these lineshapes assume a simple Poisson profile.

$$\sigma_a(\omega) = \exp(-S_j) \sum_{n=0}^{\infty} \frac{S_j^n}{n!} \delta\left(\omega - \omega_{eg} - n\omega_j\right), \tag{39a}$$

and

$$\sigma_f(\omega) = \exp(-S_j) \sum_{n=0}^{\infty} \frac{S_j^n}{n!} \delta(\omega - \omega_{eg} + 2\lambda_j + n\omega_j). \tag{39b}$$

Another interesting limiting case is when the oscillator is overdamped $\gamma_j >> \omega_j$, and the spectral density assumes the form

$$C_j''(\omega) = (2\lambda_j)\frac{\omega\Lambda_j}{\omega^2 + \Lambda_j^2}. \tag{40a}$$

with $\Lambda_j = \omega_j^2/\gamma_j$. For this case, in the high temperature limit, $\beta\hbar\Lambda_j<<1$,we get

$$g_j(t) = \left(2\lambda_j k_B T/\hbar\Lambda_j^2\right)\left[\exp(-\Lambda_j t) + \Lambda_j t - 1\right] - i(\lambda_j/\Lambda_j)\left[\exp(-\Lambda_j t) + \Lambda_j t - 1\right]. \tag{40b}$$

The nature of the lineshapes is determined by the dimensionless parameter: $\kappa_j \equiv \hbar^{1/2}\Lambda_j/(2\lambda_j k_B T)^{1/2}$. When $\kappa_j<<1$ the dynamics (with timescale Λ_j^{-1}) are slow compared with the magnitude of fluctuations (coupling strength) In this case, we can expand Eq. (40b) in a Taylor series in powers of $\Lambda_j t$, resulting in the short-time approximation $g_j(t) = \lambda_j k_B T t^2$. The absorption and fluorescence lineshapes then assume the Gaussian profiles:

$$\sigma_a(\omega) = (4\pi\lambda_j k_B T)^{-1/2}\exp[-(\omega-\omega_{eg})^2/(4\lambda_j k_B T)], \tag{41a}$$

$$\sigma_f(\omega) = (4\pi\lambda_j k_B T)^{-1/2}\exp[-(\omega-\omega_{eg}+2\lambda)^2/(4\lambda_j k_B T)] \tag{41b}$$

This is known as the *slow modulation* (static or inhomogeneous) limit. Eqs. (41) show that the Fluorescence maximum is shifted by $2\lambda_j$ to the red compared with the absorption lineshape. This Stokes Shift is an important observable in molecular photophysics and in impurity spectra in the condensed phase. In the context of electron transfer processes, λ_j is known as the solvent reorganization energy [30, 31]

In the other extreme $\kappa_j >>1$, nuclear dynamics are fast compared with the coupling strength. In this case, the exponential factors in the right-hand side of Eq.(40b) vanish very rapidly and may be ignored. At long times we have $g_j(t) = \hat{\Gamma}_j t - i\lambda_j t$, with $\hat{\Gamma}_j \equiv \lambda_j k_B T/\hbar\Lambda_j$. When this is substituted into eqs. (38), we obtain

$$\sigma_a(\omega) = \sigma_f(\omega) = \frac{1}{\pi}\frac{\hat{\Gamma}_j}{(\omega - \omega_{eg} + \lambda_j)^2 + \hat{\Gamma}_j^2}. \tag{42}$$

This is known as the *fast modulation* (homogeneous) limit [32]. In this case, the Stokes shift vanishes since the bath motions are so fast that the radiation field simply sees an averaged two-level system. Both absorption and fluorescence lineshapes assume a simple Lorentzian form with the homogeneous width $\hat{\Gamma}_j$. In summary, as κ_j

is varied, the optical absorption or fluorescence lineshapes change continuously from a Gaussian with a stokes shift of $2\lambda_j$ in the static limit to a Lorentzian with no stokes shift in the fast modulation limit.

Optical spectroscopy in solution can be interpreted using solvent spectral densities. The multimode Brownian oscillator model unifies many models and interpolates between the limits of high-frequency isolated vibrations which undergo coherent (oscillatory) motion all the way to low frequency collective overdamped solvent modes. It therefore provides a general and very convenient way for incorporating the coupling of nuclear motions to optical transitions. Spectral densities and Brownian oscillator parameters can be extracted from classical simulations. To that end, we run classical trajectories for a sufficiently long time interval $[-\tau, \tau]$. Making use of the Weiner-Khinchin and the fluctuation dissipation theorems, the spectral density is then related to the Fourier transform of the time-dependent electronic energy gap U(t) where $U(\mathbf{q}) = H_e - H_g$ [4,33],

$$C''(\omega) = \frac{1}{2\tau\hbar^2}\frac{\hbar\omega}{2k_BT}\left|\int_{-\tau}^{\tau} dt\, \exp(i\omega t)\, U(t)\right|^2 . \qquad (43)$$

In Fig. 2 we show the Brownian oscillator parameters obtained by fitting the spectral density for benzene Ar_n clusters obtained by classical simulations.

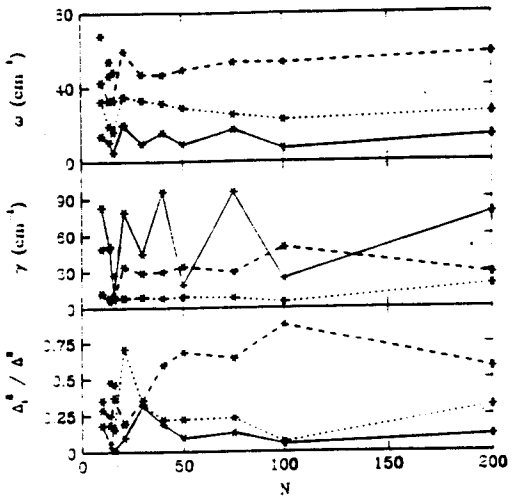

Fig. 2 Parameters for the Brownian oscillator model obtained from simulations of benzene Ar_N clusters as a function of cluster size N. A three mode model provided an excellent fit in all cases. Shown are from top to bottom the oscillator frequencies, damping and coupling to the benzene chromophor. [from L. E. Fried and S. Mukamel, Adv. Chem. Phys. 84, 435 (1993)]

The variation of these parameters with cluster size allows a systematic study of the relevant collective solvent modes and establishes the onset of bulk behavior. An

example of Raman excitation profiles calculated using the Brownian oscillator model is given in Fig. 3. This calculation allows the extraction of the solvent coupling strength λ_j and time scale (Λ_j^{-1}) from frequency-domain measurements. In Fig. 4 we illustrate the dynamics of a solvent mode as measured in pump-probe spectroscopy.

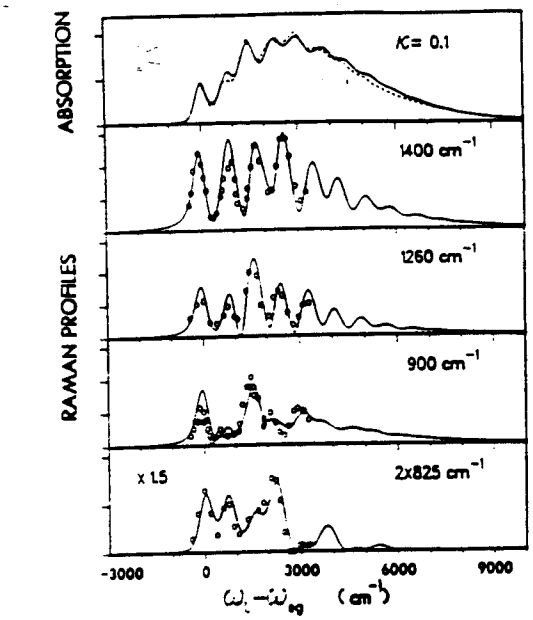

Fig. 3 *Absorption and resonance Raman profiles for azulene in CS_2 at 300 K. The solid lines are theoretical curves computed using a seven-mode stochastic harmonic model. The dashed line represents experimental data. The calculated Raman profiles (lower four panels) are compared with experiment for four different Raman transitions, as indicated [From J. Sue, Y. J. Yan, and S. Mukamel, J. Chem. Phys. 85, 462 (1986)]*

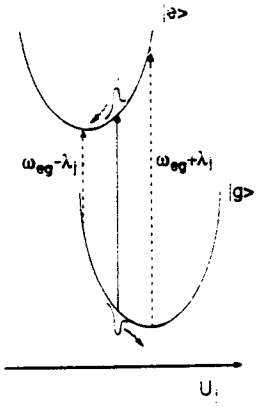

Fig. 4 *Schematic representation of pump-probe measurement and the dynamic Stokes shift for a strongly overdamped mode in the spectral diffusion limit. The potential function has a displaced equilibrium position in the ground and in the excited electronic states. Shown is the excited state "particle" and the ground-state "hole" relaxation. For the excitation wavelength shown (solid arrow)* $\omega_{eg} - \lambda < \omega_l < \omega_{eg} + \lambda$, *where* ω_l *is the pump frequency, the "particle" will show a time-dependent red shift toward the emission maximum* $\omega_{eg} - \lambda$, *and the "hole" makes blue shift to the absorption maximum at* $\omega_{eg} + \lambda$.

The pump creates an excited state particle and a ground state hole. As the delay time τ is increased, the particle and the hole undergo diffusive dynamics on their respective potential surfaces (the excited state for the particle and the ground state for the hole). The probe absorption then splits into two contributions for the particle and for the hole. This τ-dependent splitting represents the dynamic Stokes shift. At long times these terms reflect the stationary fluorescence and absorption and their splitting is $2\lambda_j$. The calculated spectrum shown in Fig. 5 clearly illustrates this behavior.

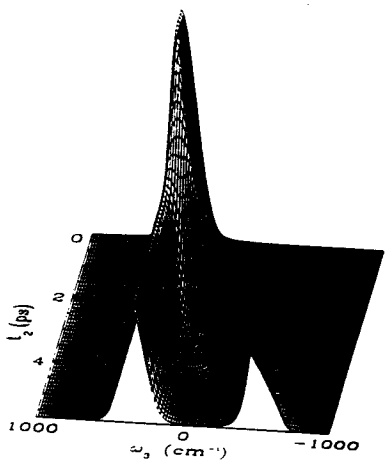

Fig. 5 *The impulsive pump-probe signal S_{pp} for an overdamped slow modulation limit Brownian oscillator shown as a function of the detection frequency ω_3 and the delay corresponds to the time-dependent Stokes shift. [from L. E. Fried and S. Mukamel, Adv. Chem. Phys. 84, 435 (1993)]*

A pump-probe measurement conducted with a spectrally narrow pump on an inhomogeneously broadened line is known as *hole burning* [34]. The name implies that the pump creates (burns) a narrow hole in the absorption lineshape, since it interacts only with a small subgroup of the ensemble. As time evolves, the system equilibrates and the hole fills. The present picture applies to *fluorescence line narrowing* experiments [35] as well (Fig. 6). In these experiments, we monitor the time and frequency resolved spontaneous emission induced by the pump. The emitted spectrum is initially narrow, reflecting the spectral selectivity of the pump, which can select a subgroup of molecules out of the inhomogeneous ensemble. The spectrum both shifts and broadens with time due to nuclear diffusive motions that are slow compared with the inverse linewidth, and that change the inhomogeneous distribution of nuclear configurations. Time and frequency resolved fluorescence of a model multimode chromophore together with the corresponding pump-probe spectra are shown in Fig. 6. The pump-probe spectrum shows both the contributions of particle and hole, whereas the fluorescence shows the hole alone.

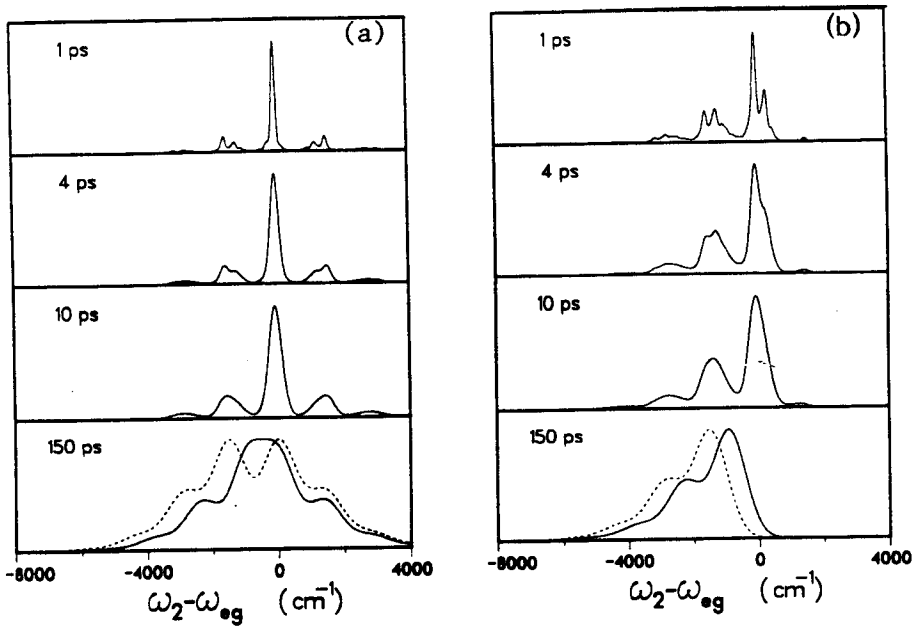

Fig. 6 *(a) Calculated hole-burning line shapes of a polyatomic solute in ethanol, following a 1 ps excitation pulse. The model solute has the 29 Raman active vibrational modes of the retinal chromophore in bacteriorhodopsin, and undergoes rapid vibrational relaxation. (b) Time-resolved fluorescence line narrowing spectra for the same system, following a 1 ps pump pulse. [From R. F. Loring, Y. J. Yan, and S. Mukamel, J. Chem. Phys. 87, 5840 (1987).]*

VII. Selective Elimination of Inhomogeneous Broadening: Photon Echoes

The linear absorption lineshape is given by a convolution of various contributions. In many cases, the electronic transition frequency ω_{eg} has a static distribution. The resulting inhomogeneous linewidth is often much broader than all other features in the spectrum. Consequently, most useful structural and dynamic information is hidden underneath this broad envelope, and may not be extracted out of the linear absorption spectrum. This is typical for spectra in solutions, liquids, glasses, proteins and molecular crystals. Since homogeneous and inhomogeneous contributions enter the linear response in a symmetric fashion (a convolution in the frequency domain or a product in the time domain) then, by definition, linear optical measurements cannot distinguish between them. If one assumes a certain profile for each of the contributions, it may become possible to obtain both contributions by a deconvolution of the lineshape. Such procedures are subjective and rely on the model

used for the system; e.g., assuming a Lorentzian homogeneous profile and a Gaussian inhomogeneous lineshape. Moreover, their accuracy becomes poor when one of the contributions is dominant. As indicated in the previous section, hole burning and fluorescence line narrowing techniques have the capacity to probe molecular dynamics and optical dephasing processes by eliminating inhomogeneous broadening. These techniques involve a selective narrow band excitation of a subgroup of molecules, which are then monitored by measuring either the spontaneous emission (fluorescence line narrowing) or the absorption of a weak probe (hole burning). Only a small fraction of the molecules within the broad inhomogeneous distribution is selectively investigated in this case, resulting in a partial elimination of inhomogeneous broadening. In this section we shall analyze photon echo experiments in which the elimination of inhomogeneous broadening is of very different origin. In contrast to the other line narrowing techniques mentioned above, the broad-band pulsed excitation in photon echo spectroscopy is non-selective, and usually the entire inhomogeneous distribution is excited. The ability of the echo technique to eliminate inhomogeneous contributions to the signal is the result of a combined effect of two carefully designed periods of evolution where the optical inhomogeneous dephasing in the first period is exactly canceled by a rephasing process in the second period. Photon echo is an ideal time-domain technique that can be best carried out using very short (impulsive) pulses (compared with any molecular timescale vibrational periods, the timescales of homogeneous dephasing, solvent motions, inverse detunings, etc.). No frequency resolution of the light pulses is necessary. This is different from other impulsive techniques such as pump-probe spectroscopy where some spectral resolution is essential.

In a two-pulse echo measurement the system interacts with a pair of pulses with wavevectors $\mathbf{k}_1$ and $\mathbf{k}_2$. Pulse 1 comes first and pulse 2 is delayed by τ. The signal is observed in the direction $2\mathbf{k}_2 - \mathbf{k}_1$. The double-sided Feynman diagrams for a general three-pulse photon echo are given in Fig. 1 When pulses 2 and 3 coincide and setting $\mathbf{k}_2 = \mathbf{k}_3$ we obtain the two-pulse echo. For a single-mode system characterized by a very large inhomogeneous broadening, the photon echo signal is sharply peaked at $t = \tau$, and the total signal integrated over t is given by

$$S_{PE}(\tau) = \exp\left[-8g_j'(\tau) + 2g_j'(2\tau)\right]. \tag{44}$$

where $g'(t)$ is the real part of g(t) (eq. (33)). In this expression inhomogeneous broadening is totally eliminated. For a coherent vibration (Brownian oscillator with no damping $\gamma_j = 0$) this gives an oscillatory (quantum beat) signal

$$S_{PE}(\tau) = \exp\left[-4\,S_j \coth\left(\beta\hbar\omega_j/2\right)\left(1 - \cos\omega_j\tau\right)^2\right]. \tag{45}$$

For an overdamped mode, we obtain

$$S_{PE}(\tau) = \exp\left\{ -8\lambda_j k_B T/\Lambda_j \int_0^\tau d\tau_1 [1 - \exp(-\Lambda_j \tau_1)]^2 \right\}. \quad (46a)$$

This has several limiting cases. In the fast modulation (homogeneous) limit (eq. (42)) we have

$$S_{PE}(\tau) = \exp(-4\Gamma_j \tau) \quad (46b)$$

In the slow modulation limit we may expand the exponent of eq. (46a) in time to lowest non-vanishing order, resulting in

$$S_{PE}(\tau) = \exp[-(\tau/T_j)^3] \quad (46c)$$

with the characteristic decay time $T_j \equiv \left(\frac{3}{8k_B T \lambda_j \Lambda_j}\right)^{1/3}$. This time profile is a signature of spectral diffusion processes. Coherent underdamped motions thus show up in impulsive echoes as quantum beats, whereas the signatures of overdamped modes are irreversible decay.

Model calculations of two pulse echoes for four-mode Brownian oscillator system are displayed in Fig. (7) .

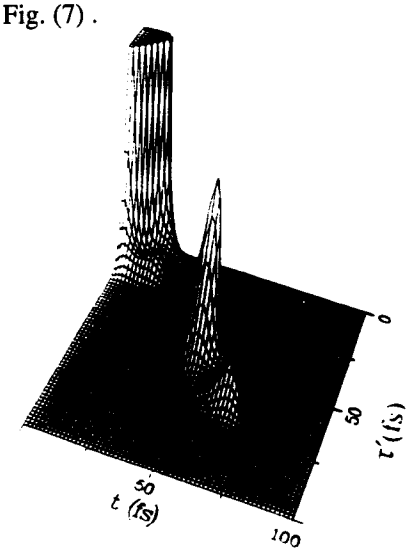

Fig. 7 *Photon-echo signal plotted as a function of the observation time t and the delay time τ, for a four-mode system. We see an initial decay, followed by oscillations (quantum beats) resulting from the modulation of the electronic polarization by vibronic coherences. Because of the inhomogeneous mode, the echo signal is centered at* $t = \tau$. *[From Y. J. Yan and S. Mukamel, J. Chem. Phys.* ***94****, 179 (1991)]*

Shown is the photon echo signal as a function of both t and τ. The echo signal is peaked at $t = \tau$. The figure shows an initial free induction decay, followed by a quantum beats resulting from the modulation of the electronic polarization by vibronic coherences. In the more general three-pulse echo, the signal is observed at $\mathbf{k}_1 - \mathbf{k}_2 - \mathbf{k}_3$, and it depends on an additional delay period (between pulses 2 and 3).

During that period the system is in a population, either in the excited state $|e\rangle$ (Fig. 1a) or in the ground state $|g\rangle$ (Fig. 1b), and undergoes spectral diffusion. The three-pulse echo thus provides additional information regarding the time-dependent Stokes shift.

VIII. Multidimensional echoes in liquids

Multiple-pulse, electronically off resonant measurements provide an effective method for probing the broad range of timescales spanned by nuclear dynamics in liquids [36]. Consider a pulse configuration consisting of a train of N pairs of simultaneous pulses, followed by a final (probe) pulse. We assume that the pulse pairs are well separated in time, and that the system is initially in thermal equilibrium in the ground electronic state. In an off resonant experiment conducted with 2N + 1 laser pulses, related to the polarizations $P^{(2N+1)}$, we need consider only N (rather than 2N) time evolution periods, in which the system is in the ground state. The third order polarization for the present pulse configurations is given by [37]

$$P^{(3)}(t) = \int_{-\infty}^{t} d\tau \, \langle i/\hbar \, [\alpha(t), \alpha(\tau)] \rangle \; E(t) \, E^2(\tau), \tag{47a}$$

where $\alpha(t)$ represents the operator $\alpha(\mathbf{q})$ in the interaction picture at time t(See eq. (16)).
The higher order polarizations are similarly given by

$$P^{(5)}(t) = \int_{-\infty}^{t} d\tau_2 \int_{-\infty}^{\tau_2} d\tau_1 \langle (i/\hbar)^2 [\, [\alpha(t), \alpha(\tau_2)], \alpha(\tau_1)] \rangle E(t) \, E^2(\tau_2) \, E^2(\tau_1), \tag{47b}$$

$$P^{(7)}(t) = \int_{-\infty}^{t} d\tau_3 \int_{-\infty}^{\tau_3} d\tau_2 \int_{-\infty}^{\tau_2} d\tau_1 \; E(t) E^2(\tau_3) \, E^2(\tau_2) \, E^2(\tau_1)$$

$$\langle (i/\hbar)^3 \, [\, [\, [\alpha(t), \alpha(\tau_3)], \alpha(\tau_2)], \alpha(\tau_1)] \rangle. \tag{47c}$$

We shall now demonstrate how such measurements can be effectively used to monitor the microscopic nature of spectral densities in liquids [36]. To that end, we consider a multimode Brownian oscillator model with a nonlinear coupling to the radiation field (i.e., through the nonlinear dependence of the transition dipole on nuclear coordinates). We assume that the electronic polarizability has an exponential dependence on the nuclear coordinate; i.e., $\alpha(q) = \alpha_0 \exp\left(\sum_j \omega_j \, \delta_j \, q_j\right)$. Here q_j are the optically active modes that couple to the electronic polarizability, and δ_j is the coupling strength. This gives

$$\langle \alpha(\tau_1) \, \alpha(\tau_2) \rangle = \alpha_0^2 \exp\,[g(0) + g(\tau_{21})], \tag{48a}$$

with the spectral function

$$g(t) = \int_0^\infty d\omega\, C''(\omega)[\coth(\beta\hbar\omega/2)\cos(\omega t) - i\sin(\omega t)], \tag{48b}$$

and the spectral density

$$C''(\omega) = \sum_j \frac{\hbar\delta_j^2}{2m_j}[\delta(\omega - \omega_j) - \delta(\omega + \omega_j)]. \tag{48c}$$

Here we have defined $\tau_{ij} \equiv \tau_i - \tau_j$. For the higher order correlation function we have

$$\langle\alpha(\tau_1)\,\alpha(\tau_2)\,\alpha(\tau_3)\rangle = \alpha_0^3 \exp\{3/2\ g(0) + g(\tau_{21}) + g(\tau_{32}) + g(\tau_{31})\}, \tag{49a}$$

$$\langle\alpha(\tau_1)\,\alpha(\tau_2)\,\alpha(\tau_3)\,\alpha(\tau_4)\rangle = \alpha_0^4 \exp\{2g(0) + g(\tau_{21}) + g(\tau_{32}) + g(\tau_{43}) + g(\tau_{31}) + g(\tau_{42}) + g(\tau_{41})\} \tag{49b}$$

The effect of different slowly interconverting or static local environments can be incorporated into this model by averaging the multitime correlation functions of α over the inhomogeneous distribution of the static degrees of freedom $W(\Gamma)$. For the two-time correlation function entering $P^{(3)}$, we have [33]

$$\langle\alpha(t)\,\alpha(0)\rangle = \int d\Gamma\, W(\Gamma)\,\alpha_0^2(\Gamma)\exp[g(0;\Gamma) + g(\tau_{21};\Gamma)]. \tag{50}$$

Similar expressions apply for the higher order polarizations. The important point is that the Γ averaging is carried out at the end; we first exponentiate, then average. This order is reserved for the homogeneous average over $C''(\omega)$. As an example, for the multimode Brownian oscillator model, Γ can include the parameters of the model, namely the strength of the dipole interaction (η_j), the frequency (ω_j), and the relaxation rage (γ_j) of the j'th mode. This model can be used to represent specific coordinates, whether local (e.g., intramolecular) or collective in nature.
Developments of femtosecond techniques made it possible to probe intermolecular vibrations in the frequency range 0 - 1000 cm^{-1} using an impulsive excitation with pulses short compared with the vibrational periods [38-41]. Under these conditions the time-resolved signal shows the coherent vibrations as well as their dephasing. Femtosecond four wave mixing measurements in liquids have yielded spectral densities which provide characteristic signatures of intermolecular nuclear degrees of freedom. Nuclear motions in liquids typically span a broad range of time scales, and vibrational lineshapes cannot be simply classified as either homogeneous or inhomogeneous. Even when such classification is possible by virtue of separation of timescales, it is not easy to firmly establish it experimentally [42]. The spectral density obtained in $P^{(3)}$ measurements contains the combined effect of an homogeneous contribution $g(\tau_{21};\Gamma)$ and an inhomogeneous distribution $W(\Gamma)$. It is

impossible to separate these contributions in a $P^{(3)}$ measurement. To illustrate this, let us calculate the response function of an oscillator with frequency ω_0. To lowest order in δ we then have

$$\left\langle \frac{i}{\hbar}[\alpha(\tau_1), \alpha(\tau_2)] \right\rangle = \frac{\alpha_0^2 \delta^2 \omega_0}{m} \langle \sin(\omega_0 \tau_{12}) \rangle_a. \tag{51}$$

The subscript a indicates the type of averaging. In the purely homogenous case we have

$$\langle \sin(\omega_0 \tau_{12}) \rangle_H \equiv \int_0^\infty d\omega_0 \, C''(\omega_0) \sin(\omega_0 \tau_{12}). \tag{52a}$$

Assuming a single oscillator with inhomogeneous broadening, we have

$$\langle \sin(\omega_0 \tau_{12}) \rangle_I \equiv \int_0^\infty d\omega_0 W(\omega_0) \sin(\omega_0 \tau_{12}). \tag{52b}$$

Since the homogeneous ($C''(\omega_0)$) and inhomogeneous ($W(\omega_0)$) distributions enter this response function in an identical fashion, it is impossible to tell them apart. Assuming that both mechanisms coexist, there are an infinite number of choices of W and C'' that will fit a given third-order signal. Higher order techniques related to $P^{(5)}$, $P^{(7)}$, etc. could provide this additional information. By looking at the joint dynamics of N evolution periods, we have in effect an N dimensional spectroscopy. This is reminiscent of two-dimensional NMR spectroscopy, which has proven extremely valuable in the analysis of complex systems such as proteins [43]. To show this, we consider the $P^{(5)}$ response function for the same model. In the homogeneous case, we have

$$\left\langle \left(\frac{i}{\hbar}\right)^2 [[\alpha(\tau_1), \alpha(\tau_2)], \alpha(\tau_3)] \right\rangle$$
$$= \frac{\alpha_0^3 \delta^4 \omega_0^2}{m^2} [\langle \sin(\omega_0 \tau_{12}) \rangle_H \langle \sin(\omega_0 \tau_{23}) \rangle_H + \langle \sin(\omega_0 \tau_{12}) \rangle_H \langle \sin(\omega_0 \tau_{13}) \rangle_H] \tag{53a}$$

In the inhomogeneous case, we obtain

$$\left\langle \left(\frac{i}{\hbar}\right)^2 [[\alpha(\tau_1), \alpha(\tau_2)], \alpha(\tau_3)] \right\rangle$$
$$= \frac{\alpha_0^3 \delta^4 \omega_0^2}{m^2} [\langle \sin(\omega_0 \tau_{12}) \sin(\omega_0 \tau_{23}) \rangle_I + \langle \sin(\omega_0 \tau_{12}) \sin(\omega_0 \tau_{13}) \rangle_I]. \tag{53b}$$

Note that τ_j are the actual times of interactions with the fields. Eq. (53a), which depends on the time delays or their sums, but not on a difference of time delays, does not show an echo. This is not the case once inhomogeneous broadening is included (eq. (53b)) where photon echoes can be clearly seen. As an example, let us take $C''(\omega_0)$ and $W(\omega_0)$ to have the form of a weakly damped Brownian oscillator with $\gamma << \omega_0$. We then have

$$\langle \sin(\omega_0 t_1)\rangle_H \langle \sin(\omega_0 t_2)\rangle_H = \exp[-\gamma(t_1+t_2)]\left(\cos[\omega_1(t_1-t_2)] - \cos[\omega_1(t_1+t_2)]\right) \quad (54a)$$

and

$$\langle \sin(\omega_0 t_2)\sin(\omega_0 t_2)\rangle_I = \cos[\omega_1(t_1-t_2)]\exp[-\gamma|t_1-t_2|] - \cos[\omega_1(t_1+t_2)]\exp(-\gamma(t_1+t_2)) \quad (54b)$$

with $\omega_1 \equiv \sqrt{\omega_0^2 - \gamma^2/4}$. The first term in eq. (53b) is an echo which shows up when the second delay period (t_2) coincides with the first (t_1).

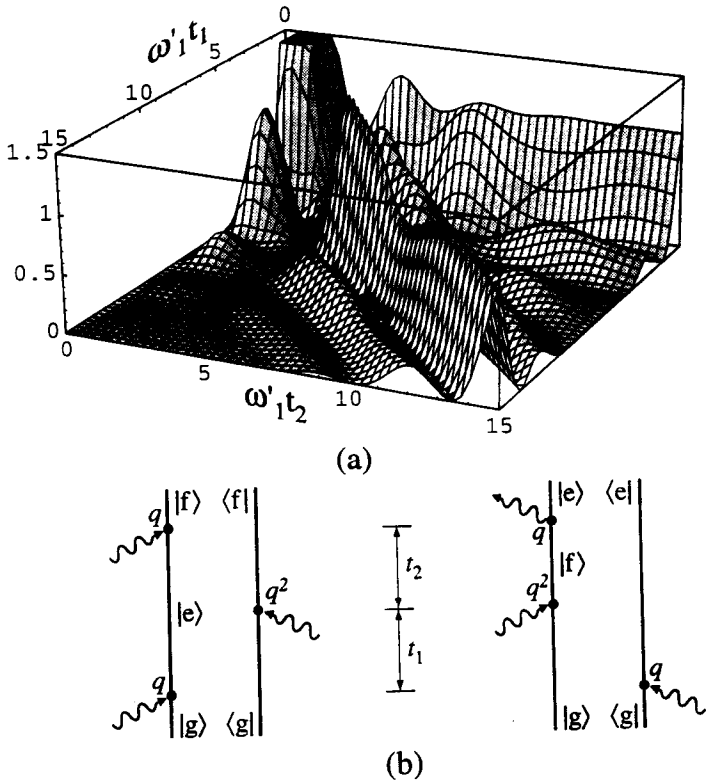

Fig. 8
(a) The fifth order response $|P^{(5)}|^2$ *calculated using an inhomogeneously broadened spectral density. (b) Double-sided Feynman diagrams representing the terms that produce the echo signal at* $t_1 = t_2$. t_1 *and* t_2 *are the delay periods between pulses.*
(From V. Khidekel and S. Mukamel, *Chem. Phys. Lett.* **240**, 304 (1995))

If $\alpha(\mathbf{q})$ were to depend linearly on nuclear coordinates, the present model would have been linear, and all nonlinear response functions should vanish identically. This can be easily seen from the Heisenberg equation for $\mathbf{q}$. In Liouville space this linearity is a result of a destructive interference of various nonlinear paths. The absence of an δ^3 term in eq. (53) reflects the destructive interference that eliminates the nuclear response for the linear model.

In Fig. 8a, we display the absolute squared value of the fifth order impulsive signal $|p^{(5)}|^2$ as a function of the delay periods t_1 and t_2 between the pulses, assuming an inhomogeneous distribution of frequencies.

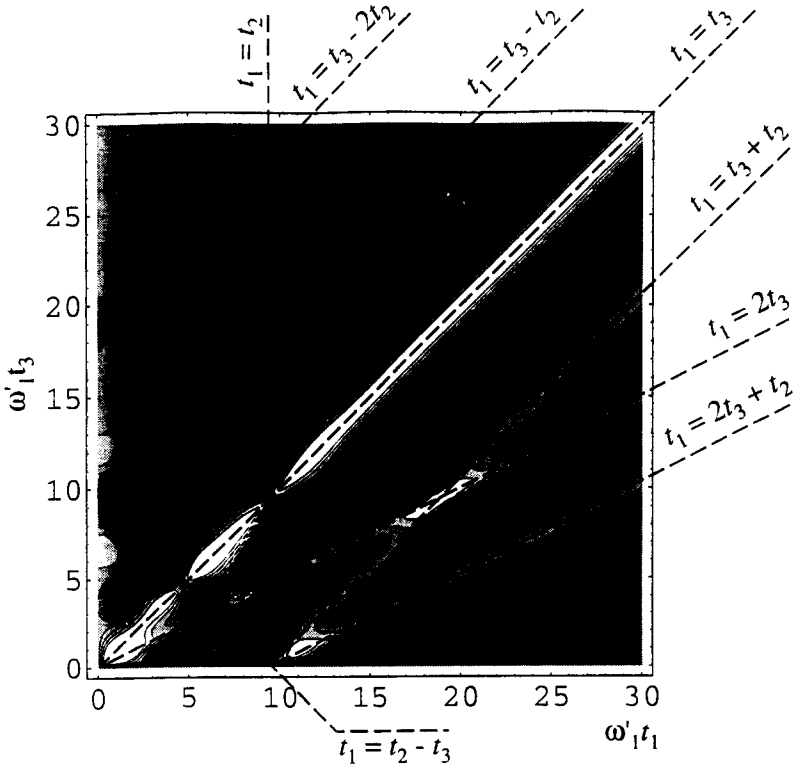

Fig. 9 *The seventh order response $|P^{(7)}|^2$ for the same model of Fig. 8. Eight distinct echo signals are clearly seen. t_1, t_2, and t_3 are the delays between successive pulses.*

A clear echo is seen at $t_1 = t_2$. The corresponding double-sided Feynman diagrams are shown in Fig. 8b. The seventh-order response function shows a similar behavior. In the general case, eight photon echo signals can be identified as shown in fig. 9. The effects predicted here, namely the appearances of echoes at specific combinations of time intervals, are very general, and are not limited to the particular model used. A major difficulty in this type of experiment is to satisfy the phase-matching condition. This is crucial in order to distinguish between various nonlinear signals that appear in closely lying directions.

ACKNOWLEDGMENTS:

The support of the National Science Foundation and the U. S. Air Force Office of Scientific Research is gratefully acknowledged. I wish to thank my students and co-workers who made invaluable contributions to the work covered in this article. Particular thanks go to R. F. Loring, Y. J. Yan, L. E. Fried, Y. Tanimura, V. Khidekel and V. Chernyak.

REFERENCES:

[1] N. Bloembergen, *Nonlinear Optics* (Benjamin, New York) (1965).
[2] S. Mukamel, *Principles in Nonlinear Optical Spectroscopy*, Oxford University Press (New York) (1995)
[3] S. Mukamel, *Phys. Reports*, **93**, 1 (1982); S. Mukamel, *Phys. Rev. A* **28**, 3480 (1983).
[4] S. Mukamel, *J. Chem. Phys.*, **77**, 173 (1982); *J. Phys. Chem.*, **89**, 1077 (1985).
[5] S. Mukamel and R. F. Loring, *J. Opt. Soc. Am. B*, **3**, 595 (1986).
[6] R. F. Loring, Y. J. Yan and S. Mukamel, *Chem. Phys. Lett.* **135**, 23(1987); *J. Chem. Phys.* **87**, 5840-(1987).
[7] Y.J. Yan, L.E. Fried and S. Mukamel, *J. Phys. Chem.* **93**, 8149 (1989); L.E. Fried and S. Mukamel, *J. Chem. Phys.* **93**, 3063 (1990)..
[8] D. J. Kane and R. Trebino, *IEEE J. Quant. Electr.* **29**, 571 (1993); J. Paye, *IEEE J. Quant. Electr.* **28**,2262 (1992
9] B. Kohler, J. L. Krause, F. Raksi, C. Rose-Petruck, R. M. Whitnell, K. R. Wilson, V. V. Yakovlev, Y. Yan and S. Mukamel, *J. Phys. Chem.* **97**, 12602 (1993).
[10] S. Mukamel, C. Ciordas-Ciurdariv, and V. Khidekel, *IEEE J. of Quant. Electr.* **32**, 1278(1996).
[11] J. Von Neumann, *Mathematical Foundations of Quantum Mechanics* (Princeton University Press, Princeton, New Jersey) (1955)
[12] U. Fano, *Rev. Mod. Phys.* **29**, 74 (1957)
[13] R. Zwanzig, *Lect. in Theoret. Phys.* **3**, 106 (1961); *Physica* **30**, 1109 (1964).
[14] M. Hillery, R. F. O'Connell, M. O. Scully, and E. P. Wigner, *Phys. Rep.* **106**, 11 (1984); K. Imre, E. Ozizmir, M. Rosenbaum, and P. E. Zweifel, *J. Math. Phys.* **8**, 1097 (1967).

[15] M. J. Rosker, M. Dantus, and A. H. Zewail, *Science* **241**, 1200 (1988); L. R. Khundkar and A. H. Zewail, *Ann Rev. Phys. Chem.* **41**, 15 (1990); A. H. Zewail, *Faraday Discuss. Chem. Soc.* **91**, 207 (1991).

[16] J. H. Glownia, J. A. Misewich, and P. P. Sorokin, *J. Chem. Phys.* **92**, 3335 (1990); R. E. Walkup, J. A. Misewich, J. H. Glownia, and P. P. Sorokin, *J. Chem. Phys.* **94**, 3389 (1991).

[17] M. Cho, S. J. Rosenthal, N. F. Scherer, L. D. Ziegler, and G. R. Fleming, *J. Chem. Phys.* **96**, 5033 (1992); N. F. Scherer, L. D. Ziegler, and G. R. Fleming, *J. Chem. Phys.* **96**, 5544 (1992); N. F. Scherer et al., *J. Chem. Phys.* **96**, 4180 (1992); M. Cho, G. R. Fleming, and S. Mukamel, *J. Chem. Phys.* **98**, 5314 (1993).

[18] C. H. Brito-Curz, R. L. Fork, W. H. Knox, and C. V. Shank, *Chem. Phys. Lett.* **132**, 341 (1986); R. A. Mathies, C. H. Brito Cruz, W. T. Pollard, and C. V. Shank, *Science* **240**, 777 (1988); H. L. Fragnito, J. Y. Bigot, P. C. Becker, and C. V. Shank, *Chem. Phys. Lett.* **160**, 101 (1989) P. C. Becker, R. L. Fork, C. H. Brito-Cruz, J. P. Gordon, and C. V. Shank, *Phys. Rev. Lett.* **60**, 2462 (1988).

[19] E. J. Nibbering, D. A. Wiersma, and K. Duppen, *Chem. Phys.* **183**, 167 (1994); *Phys. Rev. Lett.* **66**, 2464 (1991)]; K. Duppen, F. de Haan, E. J. Nibbering, and D. A. Wiersma, *Phys. Rev. A* **47**, 5120 (1993)

[20] Y. J. Yan and S. Mukamel, *J. Chem. Phys.*, **88**, 5735 (1988); S. Mukamel and Y. J. Yan, *Adv. Chem. Phys. 73*, 579-604 (1988); Y. J. Yan and S. Mukamel, *J. Chem. Phys.*, **89**, 5160 (1988).

[21] W.B. Bosma, Y.J. Yan and S. Mukamel, *Phys. Rev. A* **42**, 6920 (1990); Y.J. Yan and S. Mukamel, *Phys. Rev. A* **41**, 6485 (1990); S. Mukamel, *Ann. Rev. Phys. Chem.* **41**, 647 (1990); W.B. Bosma, S. Mukamel, B.I. Greene, and S. Schmitt-Rink, *Phys. Rev. Lett.* **68**, 2456 (1992).

[22] S. Mukamel, *J. Chem. Phys.* **82**, 5398 (1985); J. Sue, Y. J. Yan, and S. Mukamel, *J. Chem. Phys.* **85**, 462 (1986); Y. J. Yan and S. Mukamel, *J. Chem. Phys.* **86**, 6085 (1987); S. Mukamel, *Adv. Chem. Phys. 70*, Part I, 165 (1988); S. Mukamel and Y.J. Yan, *Recent Trends in Raman Spectroscopy*, S.B. Banerjee and S.S. Jha, Editors, World Scientific, Singapore (1989) p.160.

[23] L. Mandel and E. Wolf , *Optical Coherence and Quantum Optics* (Cambridge University Press, London) (1995).

[24] S. Mukamel, V. Khidekel, and V. Chernyak, *Phys. Rev. E* (Rapid Commun.) **53**, 1 (1996).

[25] P. C. Martin, *Measurements and Correlation Functions* (Gordon and Breach, New York) (1968)

[26] A. R. Bogdan, M. W. Downer, and N. Bloembergen, *Phys. Rev. A* **24**, 623 (1981); L. Rothberg, in *Progress in Optics*, Vol. 24, E. Wolf, Ed. (North-Holland, Amsterdam, 1987), p. 38; J. R. Andrews and R. M. Hoschstrasser, *Chem. Phys. Lett.* **82**, 381 (1981)

[27] M. A. Sepulveda and S. Mukamel, *J. Chem. Phys.* **102**, 9327 (1995).

[28] A. O. Caldeira and A. J. Leggett, *Physica* **121A**, 587 (1983); A. J. Leggett, S. Chakravarty, et al., *Rev. Mod. Phys.* **59**, 1 (1987); H. Grabert, P. Schramm, and G. L. Ingold, *Phys. Rep.* **168**, 115 (1988).

[29] Y. Tanimura and S. Mukamel, *Phys. Rev. E* **47**, 118 (1993); V. Chernyak and S. Mukamel, *J. Chem. Phys.* **105**, 4565-4583 (1996).
[30] R. A. Marcus and N. Sutin, *Biochim. Biophys. Acta* **811**, 265 (1985)
[31] S. Mukamel and Y. J. Yan, *Acc. Chem. Res.* **22**, 301 (1989); Y. J. Yan and S. Mukamel, *J. Phys. Chem.* **93**, 6991 (1989); Y. Tanimura and S. Mukamel, *J. Chem. Phys.* **101**, 3049 (1994).
[32] R. Kubo, in *Fluctuation Relaxation and Resonance in Magnetic Systems*, D. Ter Haar, Ed. (Oliver and Boyd, Edinburgh) (1962); R. Kubo, *Adv. Chem. Phys.* **15**, 101 (1969).
[33] L.E. Fried and S. Mukamel, *Adv. Chem. Phys.* **84**, 435 (1993).
[34] J. Friedrich and D. Haarer, *J. Chem. Phys.* **76**, 61 (1982); S. Volker, *Annu. Rev. Phys. Chem.* **40**, 499 (1989); L. R. Narasimhan, K. A. Littau, D. W. Pack, Y. S. Bai, A. Elschner, and M. D. Fayer, *Chem. Rev.* **90**, 439 (1990).
[35] M. Orrit, J. Bernard, and R. I. Personov, *J. Phys. Chem.* **97**, 10256 (1993).
[36] Y. Tanimura and S. Mukamel, *J. Chem. Phys.*, **99**, 9496 (1993); V. Khidekel and S. Mukamel, *Chem. Phys. Lett.* **240**, 304 (1995).
[37] R. W. Hellwarth, *Progr. Quant. Electron.* **5**, 2 (1977)
[38] C. Kalpouzos, D. McMorrow, W. T. Lotshaw, and G. A. Kenney-Wallace, *Chem. Phys. Lett.* **155**, 240 (1989); **150**, 138 (1988); D. McMorrow and W. T. Lotshaw, *J. Phys. Chem.* **95**, 10395 (1991).
[39] A. M Weiner, D. E. Leaird, G. P. Wiederecht, and K. A. Nelson, *Science* **247**, 1317 (1990); K. A. Nelson and E. P. Ippen, *Adv. Chem. Phys.* **75**, 1 (1989); Y. X. Yan, L. T. Cheng, and K. A. Nelson, *Advances in Nonlinear Spectroscopy*, R. J. H. Clark and R. E. Hester, Eds. (Wiley, New York) (1988), p. 299.
[40] N. F. Scherer, L. D. Ziegler, and G. R. Fleming, *J. Chem. Phys.* **96**, 5544 (1992); M. Cho, G. R. Fleming, and S. Mukamel, *J. Chem. Phys.* **98**, 5314 (1993).
[41] M. Cho, G. R. Fleming, S. Saito, I. Ohmine and R. M. Stratt, *J. Chem. Phys.* **100** 6672 (1994)
[42] R. F. Loring and S. Mukamel, *J. Chem. Phys.* **83**, 2116 (1985).
[43] R.R. Ernst, G. Bodenhausen and A. Wokaun, *Principles of Nuclear Magnetic Resonance in One and Two Dimensions* (Clarendon, Oxford, London) (1987); U. Haeberlen, *Advances in Magnetic Resonance*, Suppl. I (Academic Press, New York) (1976).